ACS APPLIED MATERIALS & INTERFACES

Letter

www.acsami.org

Pulsed-Laser Deposition of Nanostructured Iron Oxide Catalysts for Efficient Water Oxidation

Michele Orlandi,*[,†] Stefano Caramori,[‡] Federico Ronconi,[‡] Carlo A. Bignozzi,[‡] Zakaria El Koura,[†] Nicola Bazzanella,[†] Laura Meda,[§] and Antonio Miotello[†]

[†]Dipartimento di Fisica, Università degli Studi di Trento, I-38123 Povo (Trento), Italy

[‡]Dipartimento di Scienze Chimiche e Farmaceutiche, Università degli Studi di Ferrara, Via Fossato di Mortara 17-19, 44100 Ferrara, Italy

[§]Istituto ENI Donegani per le Energie Non Convenzionali, Via Fauser 4, 28100 Novara, Italy

Supporting Information

ABSTRACT: Amorphous iron oxide nanoparticles were synthesized by pulsed-laser deposition (PLD) for functionalization of indium–tin oxide surfaces, resulting in electrodes capable of efficient catalysis in water oxidation. These electrodes, based on earth-abundant and nonhazardous iron metal, are able to sustain high current densities (up to 20 mA/cm^2) at reasonably low applied potential (1.64 V at pH 11.8 vs reversible hydrogen electrode) for more than 1 h when employed as anodes for electrochemical water oxidation. The good catalytic performance proves the validity of PLD as a method to prepare nanostructured solid-state materials for catalysis, enabling control over critical properties such as surface coverage and morphology.

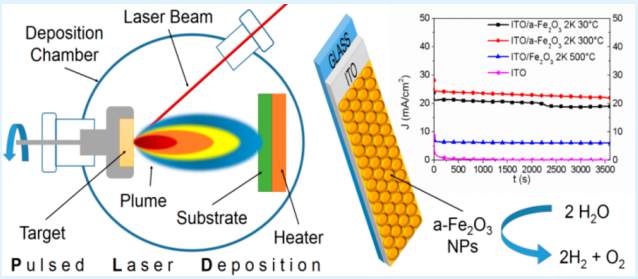

KEYWORDS: *pulsed-laser deposition, water oxidation, amorphous iron oxide, nanostructures, electrocatalysis, water splitting*

Water splitting could unlock the use of hydrogen as a clean fuel from a renewable source.[1,2] Practical application of this reaction scheme on a large scale relies upon the development of catalysts able to meet the thermodynamically and kinetically challenging requirements[3,4] posed by the half-reactions reported in eqs 1 and 2 :

$$2H_2O + 4h^+ \rightarrow O_2 + 4H^+ \qquad E^\circ = 1.23\ \text{V vs NHE} \tag{1}$$

$$4H^+ + 4e^- \rightarrow 2H_2 \qquad E^\circ = 0\ \text{V vs NHE} \tag{2}$$

where h^+ and e^- are holes and electrons, respectively. Water oxidation (eq 1), in particular, requires a large overpotential to overcome the significant kinetic barrier associated with the exchange of four electrons. Amorphous iron oxide (a-Fe_2O_3) has been identified as a suitable water oxidation catalyst, conjugating an overall good catalytic performance[5,6] in both electrolysis[7] and solar water oxidation[8] to the advantage of being earth-abundant, nontoxic, and environmentally safe.

To our knowledge, three techniques are commonly employed for the preparation of a-Fe_2O_3: successive ionic layer adsorption and reaction (SILAR),[8] electrodeposition,[9,10] and photochemical metal–organic deposition (PMOD).[7] All three methods require contact of the substrate with a solution phase. SILAR is a fast and cheap technique requiring only common laboratory glassware, which leads, however, to incomplete surface coverage and poor adhesion, and it grants no control over morphology of the deposited catalyst. Electrodeposition, which could lead to nanostructured surfaces, suffers from similar problems. PMOD is a versatile technique to obtain amorphous metal and mixed-metal oxides by spin-coating solutions of metal–organic precursors followed by UV irradiation. However, the resulting films present smooth and featureless surfaces, whereas a high roughness is generally beneficial in catalysis.

Pulsed-laser deposition (PLD) of thin films is a technique that employs high-energy-density laser pulses to generate, in the regime of phase explosion, ablated material from a solid target, consisting of a mixture of vapor/liquid nanodroplets. PLD could present some significant advantages over the methods listed above: precise control of the quantity of the deposited material, enhanced adhesion due to the energetic nature of the process, and, most importantly, the possibility of nanostructuring the surface by the deposition of nanoparticles (NPs).[11−13] Additionally, being essentially a physical deposition method, it is suitable to all kind of substrates. The main drawback of the PLD technique is the need of specialized equipment, although this is already employed in industrial applications.[14]

We report here the successful application of PLD to the synthesis of a-Fe_2O_3 NPs for functionalization of indium–tin

Received: February 18, 2014
Accepted: April 17, 2014
Published: April 17, 2014

   dx.doi.org/10.1021/am501021e | ACS Appl. Mater. Interfaces 2014, 6, 6186–6190

oxide (ITO) electrodes showing very good electrocatalytic activity toward water oxidation. ITO as a conductive substrate has been chosen for its transparency to visible light, in the perspective of extending the methodology to functionalization of silicon-based photovoltaic cells, following the approach to solar hydrogen generation proposed by Kanan and Nocera.[15,16] In such commercially available multijunction cells, ITO is commonly present as a protecting anodic conductive layer.

ITO films of thickness 350−450 nm were deposited by radio-frequency magnetron sputtering (RF-MS) of an ITO (99.99% purity) target in an Ar atmosphere (0.8 Pa working pressure) at room temperature over glass (for electrochemical and spectroscopic characterization) or silicon substrates (for electron microscopy and elemental analysis). Samples were then annealed in air at 220 °C for 2 h to increase transmittance and lower the sheet resistance (Rs) and resistivity (ρ). X-ray photoelectron spectroscopy (XPS) analysis (see Table SI1 in the Supporting Information, SI) indicates the presence of indium(III) [In $3d_4$ peak; binding energy (BE) = 444.5 ± 0.5 eV] and tin(IV) (Sn $3d_5$ peak; BE = 486.5 ± 0.5 eV) with an In/Sn ratio of 9:1 (atomic %). Grazing incidence X-ray diffraction (GIXD) reveals a crystalline phase with face-centered-cubic (fcc) structure and unit-cell parameter a = 10.16 Å (see Figure SI4 in the SI). The combined results of these analyses are definitely compatible with ITO identification. Scanning electron microscopy (SEM) was employed for thickness measurement via cross-sectional analysis and for surface imaging, revealing compact films with a polycrystalline surface (Figure SI1 in the SI). Typical values for transmittance are between 70 and 80% (400−800 nm range; see Figure SI2 in the SI) and 10−15 Ω/□ for Rs corresponding to ρ = (3.6−5.3) × 10^{-6} Ω.

The electrodes were then employed as substrates for PLD (KrF excimer laser, wavelength of 248 nm, pulse duration of 25 ns, and repetition rate of 20 Hz), with an iron disk (99.9% purity) as the target in an O_2 atmosphere (4.5 Pa working pressure). Either 2000 (2K) pulses (for working electrodes) or 6000 (6K) pulses (for GIXD characterization) of energy density (Ed) = 6.2 J/cm^2 (the choice of this value is motivated to obtain NPs, as discussed in ref 11) were applied during the deposition process, leading to layers of respectively 15 ± 5 and 60 ± 5 nm thickness, as measured by SEM cross-sectional analysis (Figure 1, top). The substrate temperature during deposition (T_{dep}) was either 30 or 300 °C. Some of the electrodes were annealed at 500 °C in air for 2 h to obtain hematite for the purpose of comparison. Iron is detected by XPS as iron(III) only (Fe 2p peak; BE = 710.5 ± 0.5 eV; see Table SI2 in the SI). SEM top-down imaging (Figure 1, bottom) reveals a structured surface, with ITO completely covered by 10−15 nm average diameter round-shaped features of homogeneous size distribution, present in all samples up to T_{dep} = 300 °C. This morphology is compatible with a NP-assembled coating.

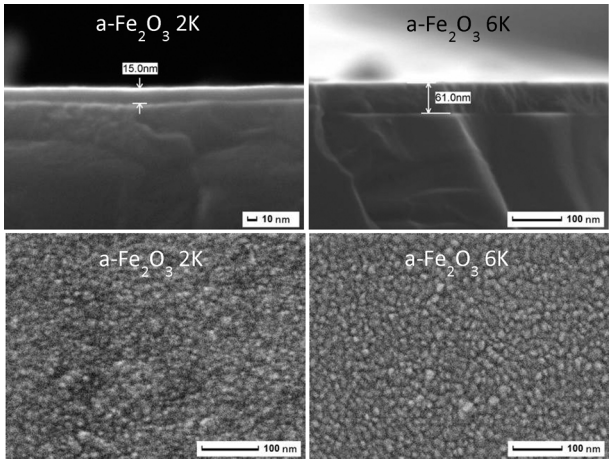

Figure 1. SEM images of a-Fe_2O_3-functionalized ITO electrode: cross section (top); top-down (bottom).

Transmittances for 2K pulses samples are between 40 and 70% (400−800 nm range; see Figure SI3 in the SI). Micro-Raman spectroscopy of 6K pulse deposition over glass substrates (Figure 2) reveals mostly an amorphous material

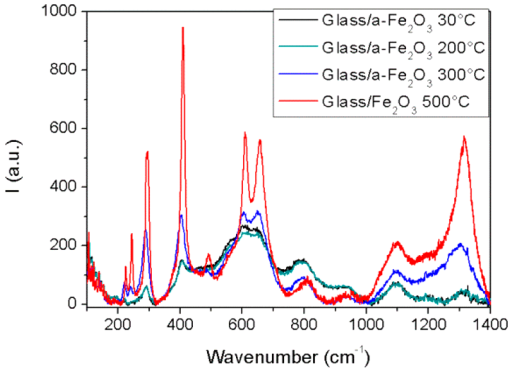

Figure 2. Micro-Raman spectra of 6K a-Fe_2O_3 deposited over glass at substrate temperatures of 30, 200, and 300 °C and of hematite-functionalized electrodes (glass/Fe_2O_3, 6K, 500 °C).

on samples up to T_{dep} = 300 °C, although a trend of increasing crystallinity with higher T_{dep} is clearly visible with this technique. Samples annealed at 500 °C in air for 2 h appear to be completely crystalline. GIXD results (Figure SI4 in the SI) on samples up to T_{dep} = 300 °C are compatible with those of a largely amorphous material, showing only a weak signal attributable to the presence of very small (6−11 nm) hematite scattering domains (hexagonal structure, unit-cell parameters a = 5.07 Å and c = 13.90 Å).

Electrochemical water oxidation experiments were performed in a three-electrode configuration, with either 2K pulse a-Fe_2O_3 or hematite-functionalized ITO as the working electrode, platinum as the counter electrode, and saturated calomel electrode (SCE) as the reference electrode. Because Fe_2O_3 is stable at pH >9,[8] a pH of 11.8 was maintained with a 0.5 M Na_2CO_3 buffer to ensure complete stability and thus well-defined electrochemistry. Oxygen evolution at this pH is expected at potential E_{O_2/H_2O} = 1.23 − (0.059pH) = 0.53 V versus reversible hydrogen electrode (RHE).[17] In Figure 3, a comparison of the anodic responses of various functionalized electrodes against bare ITO is presented. a-Fe_2O_3 shows considerable electroactivity toward water oxidation (Table 1) when deposited both at 30 °C (ITO/a-Fe_2O_3, 2K, 30 °C) and at 300 °C (ITO/a-Fe_2O_3, 2K, 300 °C) with onset overpotential η (taken at current density J = 0.2 mA/cm^2) for anodic currents of 513 and 497 mV, respectively, while hematite (ITO/Fe_2O_3, 2K, 500 °C) is only slightly less active with η = 546 mV. Though not exceptional in terms of its onset overpotential, the amorphous catalyst has a remarkably low Tafel slope, thus being able to sustain considerable current densities at moderate

dx.doi.org/10.1021/am501021e | ACS Appl. Mater. Interfaces 2014, 6, 6186−6190

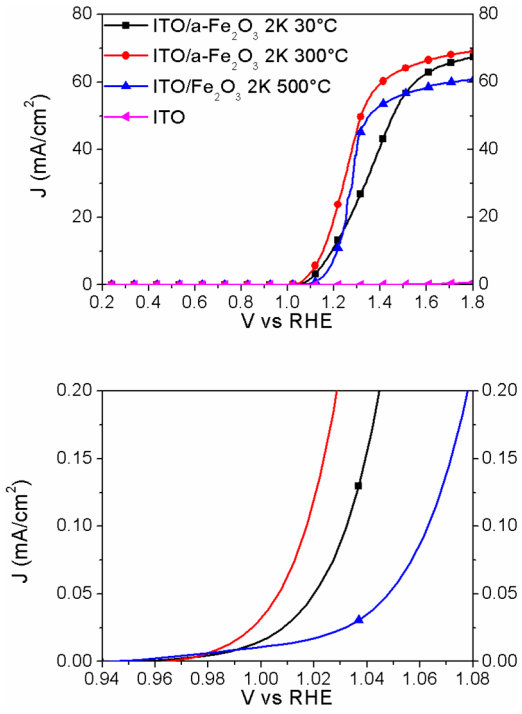

Figure 3. Linear sweep voltammetry (top) and its low overpotential magnification (bottom) of 2K a-Fe_2O_3-functionalized electrodes deposited at 30 °C (ITO/a-Fe_2O_3, 2K, 30 °C) and at 300 °C (ITO/a-Fe_2O_3, 2K, 300 °C) and of hematite-functionalized electrodes (ITO/Fe_2O_3, 2K, 500 °C). Bare ITO is reported as the reference. *J*–*V* curves compensated for the iR drop.

Table 1. Onset (J = 0.2 mA/cm^2) Overpotential η and Tafel Slope

	η (mV)	Tafel slope (mV/dec)
ITO/a-Fe_2O_3, 2K, 30 °C	513	39.7
ITO/a-Fe_2O_3, 2K, 300 °C	497	35.6
ITO/Fe_2O_3, 2K, 500 °C	546	57.3

overpotential. Indeed, where the amorphous material proves superior is in the chronoamperometries (V_{appl} = 1.64 V vs RHE for 1 h) reported in Figure 4: while hematite electrodes give

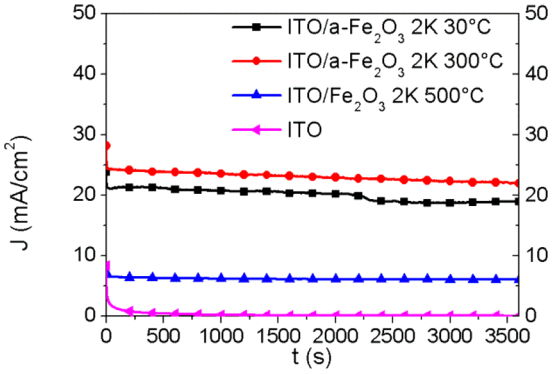

Figure 4. 1 h chronoamperometry of 2K a-Fe_2O_3-functionalized electrodes deposited at 30 °C (ITO/a-Fe_2O_3, 2K, 30 °C) and at 300 °C (ITO/a-Fe_2O_3, 2K, 300 °C) and of hematite-functionalized electrodes (ITO/Fe_2O_3, 2K, 500 °C). Bare ITO is shown as the reference. The applied potential is 1.64 V versus RHE. *J*–*t* curves did not compensate for the iR drop.

current densities of about 6.5 mA/cm^2, the amorphous material can sustain currents of more than 20 mA/cm^2, with ITO/a-Fe_2O_3, 2K, 300 °C performing slightly better (24 mA/cm^2) than ITO/a-Fe_2O_3, 2K, 30 °C (21 mA/cm^2). These current levels could be sustained without significant loss for up to 8 h (see Figure SI5 in the SI) for ITO/a-Fe_2O_3, 2K, 300 °C, while a drop in the current density accompanied by bleaching of the surface was observed for ITO/a-Fe_2O_3, 2K, 30 °C. This could be due to the loss of catalyst from the electrode surface, indicating that higher T_{dep} improves adhesion. It should be noted that a partial current drop, on the order of 30%, could be observed also in the ITO/a-Fe_2O_3, 2K, 300 °C, electrode, at the end of the 8 h chronoamperometry at 1.64 V versus RHE. Such loss does not appear to be permanent because the initial performance was reobserved on successive *J*–*V* and chronoamperometry scans (Figures SI6 and SI7 in the SI) recorded on the following days, after rinsing and storing the electrode in air under dark conditions. Thus, the partial current decrease upon prolonged electrolysis may originate by adsorption of ions, of oxidation intermediates, and of molecular oxygen, limiting the active surface of the electrode, rather than by detachment of a-Fe_2O_3, leading to permanent loss of the catalytic performances of the electrode.

Impedance spectroscopy (IS) was used for evaluating the single resistive contributions arising from different interfaces and processes. Fitting of IS was achieved with the two electric equivalents reported in Figure SI8 in the SI, where the ohmic resistance (R_1) is followed by two parallel meshes accounting for the a-Fe_2O_3/ITO (R_2 – CPE_1) and the a-Fe_2O_3/electrolyte (R_3 – CPE_2) electrochemical interfaces (Figure SI8B,C in the SI). A Warburg element (W_s1; Figure SI8C in the SI) was introduced at voltages of ≥1.14 V to account for the appearance of a diffusional arc in the complex plane plots at higher overpotentials (Figures SI9 and SI11 in the SI). In the case of the bare ITO (Figure SI8A in the SI), only one parallel element was used, corresponding to the ITO/electrolyte interface. The model describes satisfactorily the impedance response of the electrode, as shown in all cases (a-Fe_2O_3, 2K, 30, 300, and 500 °C) by the excellent agreement of the reciprocal total resistance [$R_{tot}^{-1} = (R_1 + R_2 + R_3 + R_W)^{-1}$] with the slope of the *J*–*V* curve (Figures 5 and SI17 and SI18 in the SI). The smallest charge-transfer resistance was observed for the 30 and 300 °C electrodes, showing in the core of anodic discharge ($V \geq$ 1.24 V vs RHE) charge-transfer resistances on

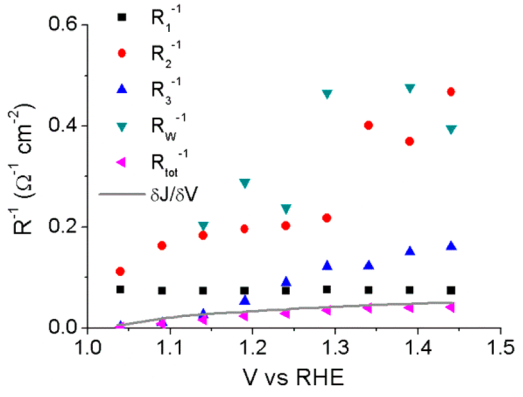

Figure 5. Reciprocal of the single resistive contributions and total reciprocal resistance R_{tot}^{-1} (magenta) compared to the derivative of the *J*–*V* curve (gray). ITO/a-Fe_2O_3, 2K, 300 °C in 0.5 M Na_2CO_3.

dx.doi.org/10.1021/am501021e | ACS Appl. Mater. Interfaces 2014, 6, 6186–6190

the order of a few ohms, comparable to the resistance of the a-Fe_2O_3/ITO interface.

In particular, it can be observed that, at potentials exceeding 1.29 V versus RHE, the charge-transfer resistance (R_3) at the interface a-Fe_2O_3/electrolyte quickly becomes significantly smaller than the constant ohmic contribution (R_1; Tables SI3−SI5 in the SI) arising from the electrolyte and ITO contact resistance; thus, after crossing the activation region, at ca. 1.00 V versus RHE, the main limitation to the anodic current density arises simply from the limited ITO conductivity. The preliminary study of the capacity of the 2K electrodes (Figure SI19 in the SI), considering the potential range from 1.04 to 1.44 V versus RHE, shows that the activity of the electrode cannot be straightforwardly related to its specific electroactive area, at least when considering the simplest model based on a parallel-plate capacitor (Tables SI6 and SI7 in the SI). Indeed, the active area of the electrodes, ca. 20 times larger than that of bare ITO, varies in the order ITO/Fe_2O_3 > ITO/a-Fe_2O_3 (30 °C) > ITO/a-Fe_2O_3 (300 °C) and does not follow the trend of the charge-transfer resistances, which decrease in the reverse order.

Although the exact mechanism of oxygen evolution at a-Fe_2O_3 catalysts is unknown, a recent study[18] on hematite photoelectrodes decorated by an amorphous iron(III) oxide catalyst resulted in enhanced hole trapping in sites capable of undergoing favorable proton-coupled electron transfer reactions, leading to the formation of highly valent Fe^{IV}=O species,[19] which may undergo subsequent nucleophilic attack by the water molecule, finally resulting in the oxygen evolution reaction. Such a reaction pathway is probable also in a thin-layer electrode, but the exact definition of the reaction intermediates remains a challenging task and requires determination of the coordination environment of the iron(III) and iron(IV) centers in the amorphous film. Such a study is currently underway.

In conclusion, we have demonstrated PLD as a valid method for functionalization of surfaces with a nanostructured a-Fe_2O_3 catalyst, obtaining electrodes that perform well toward water oxidation. With respect to other methods of preparation, PLD offers significant improvements in terms of material adhesion and control over critical parameters such as surface coverage and morphology. The methodology lends itself to the exploration of other metal oxide catalysts including mixed-metal oxides and to functionalization of other surfaces including silicon-based photovoltaic cells or other photoactive materials for solar-powered water splitting.

■ ASSOCIATED CONTENT

Supporting Information

Detailed experimental procedures, additional SEM data, XPS, UV−vis, and GIXD data for ITO and iron oxide, as well as longer chronoamperometry and in-depth IS analysis. This material is available free of charge via the Internet at http://pubs.acs.org.

■ AUTHOR INFORMATION

Corresponding Author

*E-mail: michele.orlandi@unitn.it.

Author Contributions

The manuscript was written through contributions of all authors. All authors have given approval to the final version of the manuscript.

Notes

The authors declare no competing financial interest.

■ ACKNOWLEDGMENTS

We gratefully acknowledge Claudio Cestari and Luigino Vivaldi for technical help and Dr. G. L. Marra for GIXD measurements. The research activity is partially supported by the Provincia Autonoma di Trento project ENAM in cooperation with Istituto PCB of CNR (Italy). This work was also supported by MIUR FIRB "NANOSOLAR" n. RBAP11C58Y and ENI.

■ REFERENCES

(1) Eisenberg, R.; Nocera, D. Preface: Overview of the Forum on Solar and Renewable Energy. *Inorg. Chem.* **2005**, *44*, 6799−6801.

(2) Rajeshwar, K.; McConnell, R.; Harrison, K.; Licht, S. Renewable Energy and the Hydrogen Economy. In *Solar Hydrogen Generation*; Rajeshwar, K., McConnell, R., Licht, S., Eds.; Springer: New York, 2008; Chapter 1, pp 1−16.

(3) Ruttinger, W.; Dismukes, C. G. Synthetic Water-Oxidation Catalysts for Artificial Photosynthetic Water Oxidation. *Chem. Rev.* **1997**, *97*, 1−24.

(4) Lewis, N. S. Light Work with Water. *Nature* **2001**, *414*, 589−590.

(5) Gondal, M. A.; Hameed, A.; Yamani, Z. H.; Suwaiyan, A. Production of Hydrogen and Oxygen by Water Splitting using Laser Induced Photocatalysis over Fe_2O_3. *Appl. Catal. A* **2004**, *268*, 159−167.

(6) Balu, A. M.; Pineda, A.; Yoshida, K.; Campelo, J. M.; Gai, P. L.; Luque, R.; Romer, A. A. Fe/Al Synergy in Fe_2O_3 Nanoparticles Supported on Porous Aluminosilicate Materials: Excelling Activities in Oxidation Reactions. *Chem. Commun.* **2010**, *46*, 7825−7827.

(7) Smith, R. D. L.; Prevot, M. S.; Fagan, R. D.; Zhang, Z.; Sedach, P. A.; Siu, M. K. J.; Trudel, S.; Berlinguette, C. P. Photochemical Route for Accessing Amorphous Metal Oxide Materials for Water Oxidation Catalysis. *Science* **2013**, *340*, 60−63.

(8) Cristino, V.; Berardi, S.; Caramori, S.; Argazzi, R.; Carli, S.; Meda, L.; Tacca, A.; Bignozzi, C. A. Efficient Solar Water Oxidation using Photovoltaic Devices Functionalized with Earth-abundant Oxygen Evolving Catalysts. *Phys. Chem. Chem. Phys.* **2013**, *15*, 13083−13092.

(9) Zotti, G.; Schiavon, G.; Zecchin, S.; Casellato, U. Electrodeposition of Amorphous Fe_2O_3 Films by Reduction of Iron Perchlorate in Acetonitrile. *J. Electrochem. Soc.* **1998**, *145*, 385−389.

(10) Schrebler, R.; Bello, K.; Vera, F.; Cury, P.; Munoz, E.; del Rio, R.; Gomez Meier, H.; Cordova, R.; Dalchiele, E. A. An Electrochemical Deposition Route for Obtaining α-Fe_2O_3 Thin Films Electrochemical/Chemical Deposition and Etching. *Electrochem. Solid-State Lett.* **2006**, *9*, C110−C113.

(11) Warang, T.; Patel, N.; Santini, A.; Bazzanella, N.; Kale, A.; Miotello, A. Pulsed Laser Deposition of Co_3O_4 Nanoparticles Assembled Coating: Role of Substrate Temperature to Tailor Disordered to Crystalline Phase and Related Photocatalytic Activity in Degradation of Methylene Blue. *Appl. Catal. A* **2012**, *423-424*, 21−27.

(12) Shaheen, M. E.; Gagnon, J. E.; Fryer, B. J. Laser Ablation of Iron: A Comparison between Femtosecond and Picosecond Laser Pulses. *J. Appl. Phys.* **2013**, *114*, 083110-1−083110-8.

(13) Guo, Q.; Wangzhou, S.; Liu, F.; Arita, M.; Ikoma, Y.; Saito, K.; Tanaka, T.; Nishio, M. Effects of Oxygen Gas Pressure on Properties of Iron Oxide Films Grown by Pulsed Laser Deposition. *J. Alloys Compd.* **2013**, *552*, 1−5.

(14) Gower, M. C. Industrial Applications of Laser Micromachining. *Opt. Express* **2000**, *7*, 56−67.

(15) Kanan, M. W.; Nocera, D. G. In Situ Formation of an Oxygen-Evolving Catalyst in Neutral Water Containing Phosphate and Co^{2+}. *Science* **2008**, *321*, 1072−1075.

(16) Lutterman, D. A.; Surendranath, Y.; Nocera, D. G. A Self-Healing Oxygen-Evolving Catalyst. *J. Am. Chem. Soc.* **2009**, *131*, 3838−3839.

(17) van de Krol, R. In *Photoelectrochemical Hydrogen Production*; van de Krol, R., Grätzel, M., Eds.; Springer: New York, 2012; Chapter 3, p 75.
(18) Dalle Carbonare, N.; Cristino, V.; Berardi, S.; Carli, S.; Argazzi, R.; Caramori, S.; Meda, L.; Tacca, A.; Bignozzi, C. A. Hematite Photoanodes Modified with an Fe^{III} Water Oxidation Catalyst. *ChemPhysChem* **2014**, DOI: 10.1002/cphc.201301143.
(19) Klahr, B.; Gimenez, S.; Fabregat-Santiago, F.; Bisquert, J.; Hamann, T. W. Electrochemical and Photoelectrochemical Investigation of Water Oxidation with Hematite Electrodes. *Energy Environ. Sci.* **2012**, *5*, 7626−7636.